

Evidence that Sharp Interfaces Suppress Recombination in Thick Organic Solar Cells

Obaid Alqahtani^{1,2}, Seyed Mehrdad Hosseini³, Thomas Ferron⁴, Victor Murcia¹, Terry McAfee^{4,5}, Kevin Vixie⁶, Fei Huang⁷, Ardalan Armin⁸, Safa Shoaee³, and Brian A. Collins^{1,4}*

¹Materials Science and Engineering Program, Washington State University, Pullman, WA , 99164, USA.

²Department of Physics, Prince Sattam bin Abdulaziz University, Alkharj, 11942, KSA

³Optoelectronics of Organic Semiconductors Institute, University of Potsdam, Potsdam-Golm, 14476, Germany.

⁴Department of Physics and Astronomy, Washington State University, Pullman, WA 99164, USA.

⁵Advanced Light Source, Lawrence Berkeley National Laboratory, Berkeley, CA 94720, USA.

⁶Department of Mathematics, Washington State University, Pullman, WA 99164, USA.

⁷Institute of Polymer Optoelectronic Materials and Devices, State Key Laboratory of Luminescent Materials and Devices, South China University of Technology, Guangzhou 510640, P. R. China.

⁸Department of Physics, Swansea University, Singleton Park, Swansea, Wales SA2 8PP, UK.

AUTHOR INFORMATION

Corresponding Author

*E-mail: brian.collins@wsu.edu; orcid.org/0000-0003-2047-8418

KEYWORDS: thick organic solar cells, non-Langevin charge recombination, nanomorphology, donor-acceptor interface, resonant soft X-ray scattering (RSoXS), scanning transmission X-ray microscopy (STXM), grazing incidence wide angle X-ray scattering (GIWAXS)

ABSTRACT: Commercialization and scale-up of organic solar cells (OSCs) using industrial solution printing requires maintaining maximum performance at active-layer thicknesses >400 nm – a characteristic still not generally achieved in non-fullerene acceptor OSCs. NT812:PC71BM is a rare system whose performance increases up to these thicknesses due to highly suppressed charge recombination relative to the classic Langevin model. The suppression in this system, however, uniquely depends on device processing, pointing towards the role of nano-morphology. We investigate the morphological origins of this suppressed recombination by combining results from a suite of X-ray techniques. We are surprised to find that while all investigated devices are composed of pure, similarly aggregated nanodomains, Langevin reduction factors can still be tuned from ~2 to >1000. This indicates that pure aggregated phases are insufficient for non-Langevin (reduced) recombination. Instead, we find that large well-ordered conduits and, in particular, sharp interfaces between domains appear to help to keep opposite charges separated and percolation pathways clear for enhanced charge collection in thick active layers. To our knowledge, this is the first quantitative study to isolate donor:acceptor interfacial width correlated to non-Langevin charge recombination. This new structure-property relationship will be key to successful commercialization of printed OSCs at scale.

1. Introduction

Organic solar cells (OSCs) with solution-printed active layers have attracted a great deal of attention due to their tuneable properties, mechanical flexibility, and continuously rising power conversion efficiency (PCE) in the last two decades.^{1,2} The current PCE record for OSCs is about 18%.^{3,4} In bulk heterojunction (BHJ) OSCs, where electron donating and accepting materials are blended together in a common ink, PCE usually maximizes when the thickness of the active layer is around 100 nm. As the BHJ thickness increases, light absorbance increases following an interference-induced oscillatory pattern, potentially resulting in higher current densities in the thicker junctions. However, charge recombination increases faster with increasing thickness scaling inversely with the square of the film thickness.⁵ Consequently, in most polymer-based OSCs, the device performance rapidly decreases as the BHJ thickness increases beyond the first absorbance interference peak.⁶⁻⁹ One of the existing challenges facing the industrialization of OSCs at a large scale is the difficulty of controlling and processing thin active layers.¹⁰ This is because most large-scale fabrication methods, e.g. roll-to-roll printing, can only reproducibly deposit pin-hole-free films greater than 400 nm.¹¹

The investigated system is amongst relatively few systems that maintain high efficiencies in the thick junction regime.^{10,12} The recently synthesized electron donating co-polymer, Naphtho[1,2-c:5,6-c']bis([1,2,5]-thiadiazole) based copolymer (NT812, Figure 1a bottom), exhibits PCE>10% when fabricated into OSCs with phenyl-C71-butyric acid methyl ester (PC71BM) fullerene as the electron acceptor (Figure 1a top).¹³ The novelty of NT812 appeared when this system maintained high PCE even with thick BHJ active layers $\sim 1\mu\text{m}$. It was found that at optimal fabrication conditions, bimolecular recombination is significantly suppressed up to 800x below what is expected for the diffusive Langevin model (where charges' trajectories are random and depend on the charge carrier mobilities—for more details we refer the reader to our previous work,⁷ or to original work of Langevin classical model¹⁴). This non-Langevin

behaviour leads to OSCs with less recombination losses, i.e. Shockley-type solar cells.⁷ In fact, recombination is suppressed so much in this system that its performance increases rather than decreases with thickness up to 300 nm, making it one of the highest performing systems to exhibit such favourable behaviour.¹⁵ Although non-fullerene acceptor (NFA) systems dominate performance with thin active layers, work to reduce recombination in these systems has only just begun,¹⁶ and to our knowledge no NFA systems have demonstrated such increased performance beyond the first interference maximum.

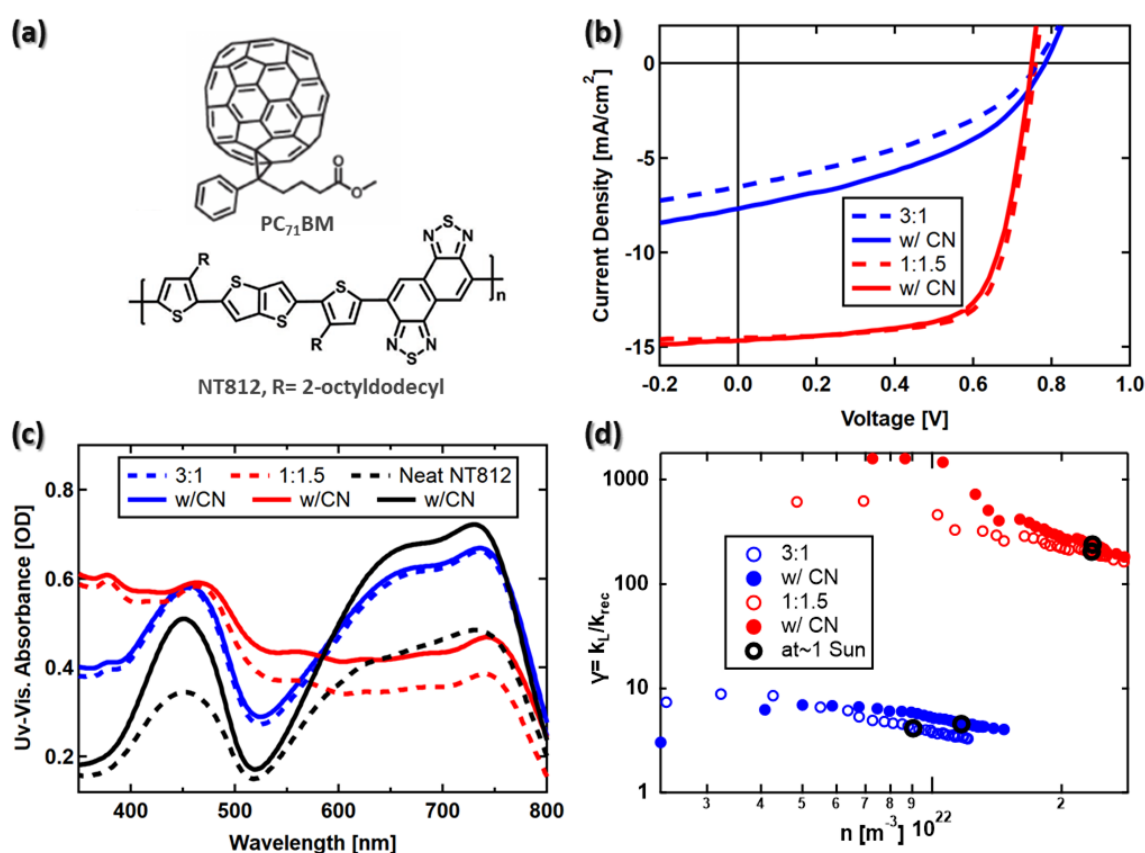


Figure 1. a) Chemical structure for the fullerene (top) and polymer (bottom). b) J-V characteristic curves for the four different solar cells. c) UV-Vis absorbance for neat polymer with and without CN as well as for all blends. d) Reduction factor of bimolecular recombination as a function of carrier density in all four NT812: PC71BM blends. Black circles show the reduction factor data points at about 1 sun.

Investigation into the origin of this phenomenon demonstrated that the charge mobilities the NT812:PC71BM system are rather mundane and cannot explain the very efficient charge

collection. A proposed scenario is either a unique interfacial charge transfer (CT) state with fast dissociation dynamics relative to the decay rate or a special morphology that allows thick non-Langevin BHJ OSCs.^{7,17} A combinatory scenario can be possible as well where improved nano-morphology enhances CT state dynamics. Importantly, one study found that nearly classical Langevin recombination could be exhibited in this system by changing the donor-acceptor ratio⁷, which indicates a morphological origin to the non-Langevin behaviour. Only a handful of other D:A combinations show similar behaviour.^{9,18,19}

General work on the topic has suggested that high crystallinity of the donor is important,^{20,21} or in the case of amorphous polymers, that relatively pure phases help by reducing charge recombination.²² Unfortunately, early experimental and computational work investigating interfacial sharpness on recombination have resulted in conflicting conclusions. While some reports suggest that sharp interfaces reduce recombination,^{23,24} others conclude that disordered or mixed interfaces are best.^{25,26} However, none of these studies directly measured bulk heterojunction interfacial properties such as interfacial sharpness. Clarke et al. compared two polymer:fullerene systems with similar nanostructure but distinct charge recombination behaviours to probe morphological origins of non-Langevin dynamics. Their transmission electron microscopy (TEM) investigation could not reveal any significant morphological difference, however, and they were not able to compare Langevin and non-Langevin recombination in the same material system.²⁷ The NT812:PC71BM system, with its ability to switch between the two behaviours, represents an opportunity to reveal the critical nanostructure leading to non-Langevin recombination but will require an advanced quantitative characterization of the nanostructure.

We have shown in our previous work that the critical morphological parameters of crystallinity, domain purity, and domain size can be measured by a strategic application of a suite of synchrotron X-ray techniques.^{28–30} Our recent work has demonstrated the capability of these techniques to additionally probe interfacial sharpness.^{30,31} The work highlighted the

importance of interfaces on charge generation but wasn't conclusive with respect to recombination. Venkatesan et al. noted reduced recombination with enhanced Kelvin probe surface potential differences between domains in blends cast from solvent additives.³² This correlated with increased domain purity, but they didn't investigate interface morphology. Another study reported evidence that rough D:A bulk heterointerfaces correlated with good exciton dissociation but did not monitor recombination.³³ Thus to date, no work has directly measured morphology including interfaces, while at the same time isolating and suppressing recombination.

In this work we apply our suite of X-ray nanoprobe to directly reveal the critical morphology behind the activation of highly suppressed non-Langevin recombination. We uniquely combine our measurements to quantify the donor-acceptor (D-A) interfacial sharpness in BHJ blends. Varying the active layer blend ratio and solvent additive content effectively switches the charge recombination dynamics between Langevin and non-Langevin in the same system, suggesting that reduced recombination is morphology driven. We are surprised to find that even our active layers exhibiting Langevin recombination are composed of pure, well-aggregated phases. Instead, we find that large domains with sharp D-A interfaces correlate with suppressed, non-Langevin recombination with reduction factors >1000, indicating these are the morphological mechanisms that enable thick and efficient active layers. Such findings can guide future research to achieve high-performing systems suitable for large-scale production of OSCs.

2. Results

OSC active layers were spin coated with a (D:A) blend *wt.* ratios of (1:1.5) and (3:1) both with and without 0.5 vol % chloronaphthalene (CN) as a solvent additive, since these conditions exhibited both Langevin and Non-Langevin recombination dynamics previously.⁷ Rather than 1 μ m thick active layers, ~200 nm active layers were investigated to enable both device physics and X-ray nanoprobe analyses on the same set of samples by the participating groups. 100 nm and 200 nm active layers revealed identical morphologies and performance scaled only by

absorption (see Figure S1, S26 and S27, SI). It is worth noting that our previous device physics investigation of thin (100 nm) and thick (800 nm) films show similar carrier mobilities in both junctions.⁷ Thus, thicker films are likely to have similar morphologies. Figure 1b displays the JV curves under AM1.5G solar illumination, and Table 1 summarizes device performance metrics, which are similar to previous reports.^{7,13} In particular, the (1:1.5) devices show about four times more efficiency than (3:1) blends with all of the improvement from the short circuit current (J_{sc}) and fill factor (FF).³⁴ Although UV-Vis spectra on pure films show some differences when adding the CN additive, no significant difference in aggregation due to CN can be detected in the blends investigated, suggesting that the polymer in all blends is well aggregated.

Figure 1d shows the reduction factor of the bimolecular recombination γ , which is the ratio of the classical Langevin recombination coefficient k_L ,¹⁴ to the coefficient k_{rec} in a given photoactive layer, $\gamma = k_L / k_{rec}$. The bimolecular recombination in the limit of a homogeneous

Table 1. Summary of device performance, reduction factors of bimolecular recombination and charge carrier mobilities in NT812:PC71BM films with different blend ratios, processed with and without solvent additive. The device performance parameters are average of 6 devices. The bimolecular recombination reduction factors ($\gamma = k_L / k_{rec}$) are calculated based on steady-state bias-assisted charge extraction measurements and the mobilities (fast and slow carriers) are calculated based on resistance-dependent photovoltage measurements (see Figure S2 and S3, SI). The listed γ values are at about 1 sun intensity. ^(a)

Blend (NT812:PC71BM)	Additive CN [vol %]	V_{oc} [V]	J_{sc} [mA.cm ⁻²]	FF [%]	Avg. PCE [%]	γ k_L/k_{rec} (a)	μ_s [cm ² V ⁻¹ s ⁻¹]	μ_f [cm ² V ⁻¹ s ⁻¹]
(3:1)	0	0.77	6.42	39	1.88(0.08)	2	2.5×10^{-4}	2.5×10^{-4}
(3:1)	0.5	0.78	7.49	41	2.43(0.06)	5	3.0×10^{-4}	3.0×10^{-4}

(1:1.5)	0	0.75	14.69	70	7.85(0.25)	200	2.2×10^{-4}	8.1×10^{-3}
(1:1.5)	0.5	0.74	14.79	69	7.67(0.13)	250	2.9×10^{-4}	9.0×10^{-3}

medium can be approximated by the Langevin recombination rate constant, which is proportional to the mean carrier mobility. This was calculated in a similar manner to our previous work (see Figure S2, SI).⁷ As expected, the (3:1) blend without the CN additive exhibits nearly classical diffusive Langevin recombination. In contrast, the (1:1.5) devices show about two orders of magnitude lower recombination coefficients with $\gamma_{max} > 1000$. The (1:1.5) devices are, therefore, considered to exhibit non-Langevin recombination dynamics. The solvent additive also improves the reduction factor (more significantly for the 3:1 blends) with all trends holding true at the operational conditions (~ 1 sun), see Table 1 and the black circles in Figure 1d.

Resistance-dependent photovoltage (RPV) transient measurements were used to separately determine faster and slower carrier mobilities in each blend. All mobilities, are unremarkable and rather typical of values in other high performing polymer:fullerene OPVs— in agreement with previous work.⁷ We were not able to separate the slower and faster carrier mobilities in the (3:1) blends, likely due to them being too similar. Importantly, there are no significant changes in mobilities due to processing conditions other than the fast carriers (typically identified as electrons in the fullerene phase)^{35,36} have increasing mobilities in the films with the better blend ratio as shown in Table 1 (also see Figure S3, SI). However, increasing electron mobilities only serves to unbalance the charge transport, and even these mobilities are still typical of polymer:fullerene blends. These results suggest that the charge extraction rate is not extraordinary, but rather the bimolecular recombination rate is low. This allows for efficient charge collection even when the film thickness increases.⁷ Contrary to mobility, γ improves by about 100 times with the blend ratio. In many other OSCs with either polymer or small molecule donors, the non-Langevin behavior has been shown to be key for maintaining high FF even at

active layer thickness ~ 300 nm.^{9,17,18,37,38} Thus, the lower FF values in (3:1) blends can be attributed to their higher biomolecular recombination in comparison to their (1:1.5) counterparts.

We now turn to morphological characterization to understand how the additive and D-A ratios can turn on and off the Langevin recombination property. We first investigate the crystallinity of the electron donor (NT812) and fullerene (acceptor) aggregates using grazing-incidence wide-angle X-ray scattering (GIWAXS) measurements. The results of the experiments on both neat and blend films are presented in Figure 2 with additional results and analysis provided in the supporting information. Figure 2a and 2b show 2D GIWAXS images for (3:1) and (1:1.5) blends, respectively, both with CN. The strong scattering ring at $q=1.36 \text{ \AA}^{-1}$ indicates the presence of pure PC71BM aggregates as evidenced by the similar ring for a pure PC71BM film. The scattering peaks at $q=0.29 \text{ \AA}^{-1}$ indicate polymer lamellar (100) stacking with only a weak second order (200) detectable. The primarily out-of-plane (OoP) peaks at $q_z=1.83 \text{ \AA}^{-1}$ represents π -stacking (010) with a face-on orientated population with respect to the substrate in addition to a randomly oriented crystal population. We focus on these face-on π -stacking peaks because this packing is favourable for charge transport. Figure 2c shows 1D GIWAXS profiles extracted from the 2D images in the OoP direction, i.e. a line cut in the vertical direction (q_z). Figure S5 and S7, in SI, show vertical and horizontal 1D profiles and peak assignments. The intensities of both peaks closely follow the blend ratio, suggesting the degree of crystallinity or aggregation is similar in all blends. Pole figures analysis of (010) supports the claim of similarity in degree of crystallinity in all blends (see Figure S9, SI). The polymer and PC71BM diffraction characteristics in all blends are consistent with their pure film counterparts and suggests the existence of both pure polymer and pure PC71BM domains in all active layers.

Results of peak width Scherrer analysis (Figure S6, SI) of the coherence length (D) are displayed in Figure 2d and Figure S8, SI—where D is a measure of length-scale ordering within

a crystal or crystal size.³⁹ In each case, the solvent additive enhances ordering in the blends by increasing D for the OoP π -stacking (Figure 2d). While there is little change in π -stacking for the (3:1) blend film, π -stacking is significantly enhanced for the (1:1.5) blends. A similar improvement occurs for electronically insulating lamellar stacking (Figure S8, SI). All blends cast with the CN additive, however, have similar π -stacking coherence lengths to the pure polymer film. The enhancement of coherence length with CN is consistent with its role as a plasticizer and the effect of the fullerene to increasingly disrupt polymer packing.⁴⁰ In contrast to the polymer packing, D of the main fullerene peaks are invariant with CN, and D in (1:1.5)

blends are equal to those in pure fullerene. (3:1) blends show similar, but smaller values of fullerene D . This suggests slightly more disordered PC71BM aggregates in (3:1) films, which is consistent with lower electron mobilities in these blends as interpreted from our RPV

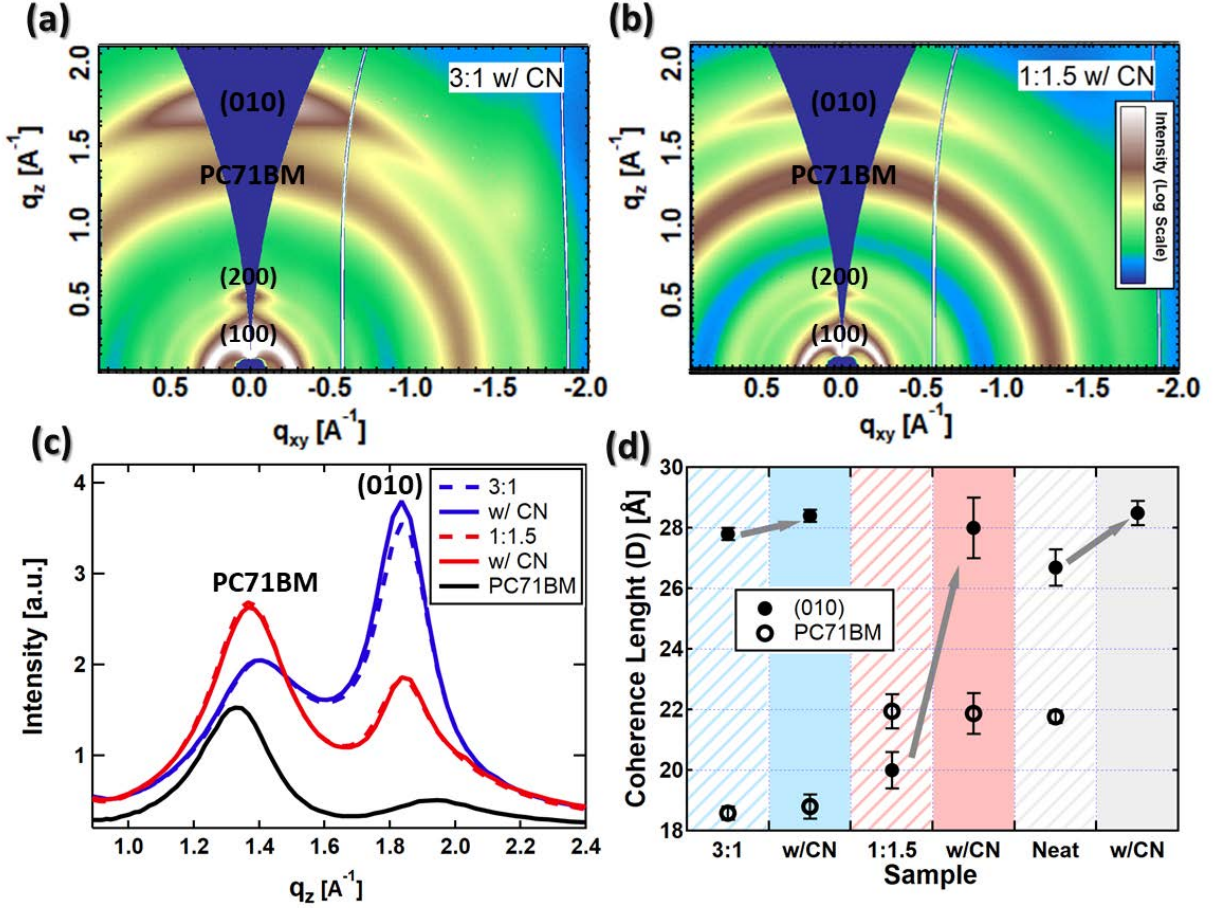


Figure 2: GIWAXS results for neat materials (NT812 and fullerene) and blends. 2D GIWAXS scattering results for NT812: PC71BM blends of (3:1) blend with CN (a) and 1:1.5 blend with CN (b). The 2D images are plotted with the same color scale of the scattering intensities [a.u.], also corrected for the missing wedge. c) 1D GIWAXS profiles extracted from the 2D images in the OoP vertical direction (q_z) for all blends. Also, the graph includes the GIWAXS profile of neat PC71BM (black) to help with peak assignments. PC71BM and (010) peaks are indicated in the graph. d) Coherence length (D) for PC71BM peak at $q_z=1.36 \text{ \AA}^{-1}$ (open circles) and (010) peak at $q_z=1.83 \text{ \AA}^{-1}$ (solid circles) in blends as well as in neat materials were calculated via Scherrer analysis (details in the Supporting Information).

experiments. Coherence length also sets a lower limit to the size of pure phases in the blends.

We cannot say much about the size of pure fullerene domains as even pure films only exhibit diffraction with $D \sim 2 \text{ nm}$ (Figure 2d). However, the polymer lamellar diffraction demonstrates $D \sim 14 \text{ nm}$ for all samples (Fig. S8, SI), making this the lower limit of pure polymer domains in the blends. From Figure S8, it is noticeable that D of the lamellar peak in neat polymer films is lower than in the blends. Although that might seem counterintuitive, there is precedent in the

literature for other systems that show similar behavior.⁴¹ We observe that as the amount of fullerene increases, the in plane lamellar peaks narrow and thus result in higher coherence length (Figure S8). Such an effect could arise from a strong drive to phase separate early during film formation, enabling more time to order.

To more accurately probe domain size, composition, and connectivity, we used scanning transmission X-ray microscopy (STXM)⁴² combined with near-edge X-ray absorbance fine structure (NEXAFS).⁴³ Figure 3 presents NEXAFS and STXM results for a (1:1.5) with CN blend with film thickness ≈ 100 nm for better clarity in the transmission mode image. The similarity of the results on this film were confirmed by identical scattering profiles between the thinner and thicker active layers (see Figure S26, SI) as well as qualitative STXM images of thicker films (Figure S16, SI). The linear fitting of NEXAFS spectra for the blend, shown in Figure 3a, confirms the average weight ratio, 40% polymer, across the film. Figure 3b presents a STXM image where dark regions represent a matrix of (50-100 nm sized) PC71BM rich domains, and the white fibrils indicate polymer rich domains that are 30-50 nm in width. These measurements are consistent with the lower limits of domain size determined from the GIWAXS analysis. The fibrillar nature of the polymer domains indicate well-connected pure crystalline polymer conduits for hole transport that are larger than the classical P3HT-based OSC fibril network. The PC71BM domains are large enough to easily connect to the electrodes—we anticipate that to hold true even in thick films. A qualitative comparison between the two blend ratios with active layers at thicknesses >200 nm (see Figure S16, SI) shows a similar fibril network with the (3:1) film exhibiting polymer fibrils with a smaller spacing due to less PC71BM loading. The spectroscopic nature of STXM imaging enables chemical mapping of the domains. Our quantitative analysis (details in Figure S12 and S13, SI) is carried out on the thinner 100 nm film, near regions likely to be mostly one domain throughout the film thickness (e.g. nodes of polymer fibrils) with an example composition line profile shown in Figure 3c (many more in

Figure S13, SI). The peaked nature of the composition profiles originates from the STXM beam size (~ 50 nm). After correcting for the X-ray beam convolution in a similar fashion to our

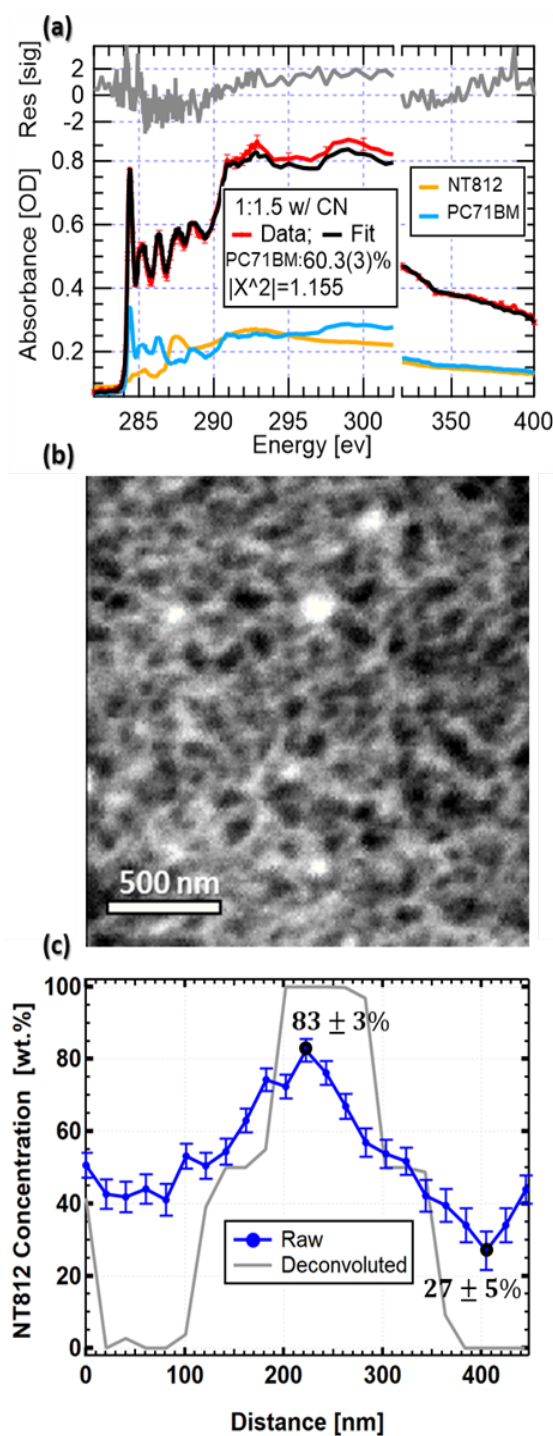


Figure 3. Morphology investigation of OPV active layer in a 100 nm thin (1:1.5) blend with CN. a) NEXAFS spectra: pure NT812 (orange), PC71BM (blue), blend (Red), and a linear combination fit of spectra for NEXAFS for pure components (black). b) STXM composition scan was acquired at 284.4 eV, which is fullerene absorption peak. PC71BM (dark regions) and NT812 (white fibrils). c) Concentration profiles of NT812 across different compositional domains; (blue) raw and (grey) deconvoluted.

previous work (details in Figure S14 and S15, SI),²⁹ the deconvoluted results indicate pure polymer and pure fullerene domains, agreeing with the GIWAXS analysis. We were not able to conduct compositional analysis on thick films due to vertically overlapping domains.

We now turn to resonant soft X-ray scattering (RSoXS) as a complement measurement of domain size and purity with the unique opportunity to also investigate D-A interfaces.⁴⁴ The Lorentz-corrected RSoXS scattering profiles in Figure 4a were strategically acquired just below the absorption edge to enhance phase contrast, limit damage, reduce orientation contrast, and eliminate X-ray fluorescence backgrounds. They show that the (3:1) blends have scattering peaks at $q=0.10\text{ nm}^{-1}$ which corresponds to a characteristic length (which determines the average center-to-center distance between scatterers and defined as $L_C = 2\pi/q^*$ where q^* is the peak position) of 62 nm. On the other hand, the (1:1.5) films show scattering peaks at $q=0.064\text{ nm}^{-1}$ and $L_C \approx 98\text{ nm}$. Although without modeling these values are only approximate, however, they are consistent with the domain spacing from STXM analyses. Given that the (3:1) blends are majority polymer, it is likely that the polymer domains in this blend are the same size as in the (1:1.5) blend. This is due to the self-limiting nature of polymer fibrils seen in most semicrystalline polymer films. Thus, a smaller characteristic length is likely due to a reduction in fullerene domain size to below 30 nm as estimated from L_C as detailed in the supporting information, part S10. CN does not affect the peak position and therefore has no impact on the characteristic length (Figure S20, SI) but does increase the scattering intensity. The insensitivity of L_C to the plasticizing CN indicates that the nanostructure is driven by crystallinity rather than liquid-liquid phase separation. Furthermore, anisotropic scattering at the X-ray energy of 285.4 eV was measured and has been interpreted as indicating a preferential molecular orientation at D-A interfaces in other systems.⁴⁵ Here the scattering anisotropy is the same sign for all blends, suggesting that the in D-A interfacial orientation does not change with processing conditions investigated and is thus not a significant factor determining performance

in this case. Additional tilted-film RSoXS measurements, conducted to express the qz component (see Figure S22)⁴⁶ were consistent with no vertical stratification and in agreement with pure domains measured in STXM that integrates the vertical film direction.

The increase in RSoXS intensity with CN suggests that the solvent additive enhances the average composition variation between the polymer and fullerene domains. The total scattering intensity (TSI) calculated by integrating the scattering profiles over all of reciprocal space (area under the profiles in Figure 4a) is proportional to the mean-squared composition difference between domains ($\Delta C_{RMS} \propto \sqrt{TSI}$, RMS is root-mean-squared).²⁹ ΔC_{RMS} was calculated on an absolute scale by combining this measurement with the STXM domain composition analysis and prior knowledge of the donor/acceptor ratio as we have done in our previous work²⁹ with details shown in Figure S17-S21, SI. Figure 4b displays the result of this analysis (y-axis) with uncertainties primarily from convolution of domain composition with volume fraction (Figure S21, SI). The ΔC_{RMS} analysis tracks the RSoXS profile intensities seen

in Figure 4a with the average domain composition fluctuation greatest for the (1:1.5) blends and with the CN additive.

There is significant evidence (from GIWAXS and STXM) that both polymer and fullerene domains are pure. However, $\Delta C_{RMS} < 100\%$ means that mixed regions of the active layer must exist somewhere. There is no clear evidence of a separate third phase in our STXM images, so the mixed region must actually be manifest as interfacial mixing in a narrow region below

the resolution limit of the microscope. Such an interpretation follows from other systems like this one where evidence of mixing with fullerenes only occurs at polymer fibril interfaces.^{30,47–}

⁴⁹ Previously we determined interfacial width in a block copolymer using absolute scattering intensity.⁴⁶ The required measurements for such analysis were not conducted here, but we can

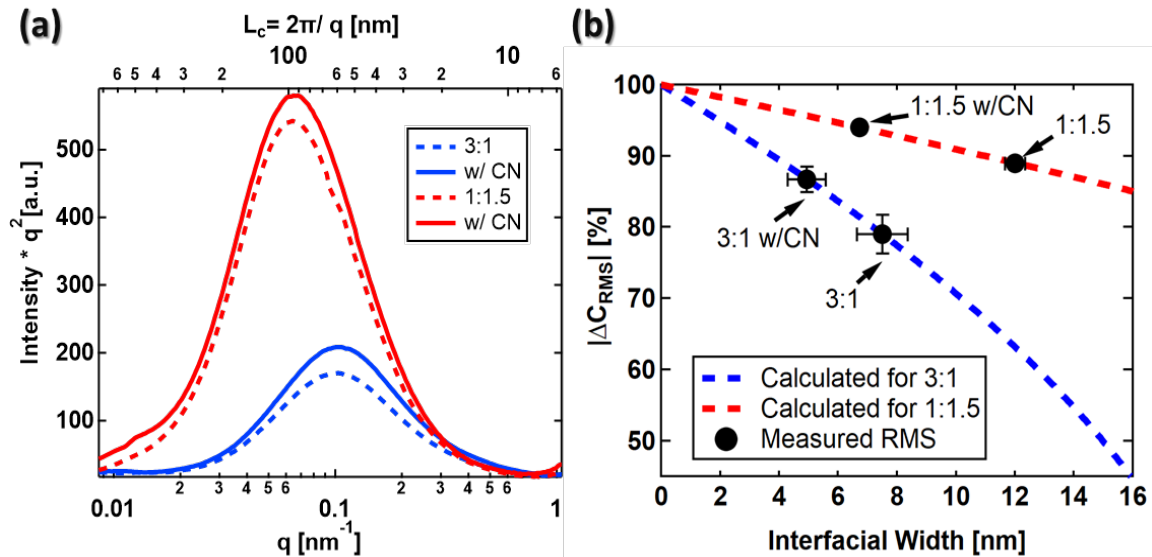


Figure 4. a) Lorentz-corrected RSoXS profiles acquired at 283.5 eV for active layers of the four investigated samples as indicated in the graph legend. b) Averaged differences in composition between different domains, based on two-domain model. The dotted lines represent the mathematically calculated ΔC_{RMS} values of composition differences as a function of the D-A interfacial width. The black circles are the extracted values of the D-A interfacial width based on STXM and RSoXS results.

instead combine ΔC_{RMS} with measurements of domain spacing and volume fraction to extract an interfacial width. In this calculation (detailed in Figure S23-S25, SI) we assume circular fibril cross-sections and a linear interfacial composition profile. This results in a simple analytic

solution for the interfacial width between pure domains, which notably makes no assumption of the packing arrangement of the fibrils and is also robust to a wide distribution of fibril sizes. The results of calculating the interfacial width are shown as the x-position of the black dots in Figure 4b. Thus, we attribute the increase of ΔC_{RMS} with CN additive to the D-A interfaces becoming sharper, with the widest interfaces at 12 nm sharpening to less than 5 nm in width. In short, the CN plasticizing solvent additive enables cleaner crystallinity-driven phase separation, sharpening the D-A interfaces.

3. Discussion

Figure 5 depicts the morphology of the investigated NT812:PC71BM active layers that is consistent with all measurement results and analysis presented above. Blue represents pure polymer fibrils in a red matrix of pure fullerene. The black bars symbolize polymer chains inside the fibrils whose packing slightly improves with the solvent additive (see coherence length measurements). Notably there is only evidence of improvement in 1:1.5 blends, but not in 3:1 blends (see also the UV-Vis spectra for 3:1 blends). The color gradient at fibril edges depicts interfacial mixing, which decrease with the CN additive, thus making the domain interfaces sharper (and increasing ΔC_{RMS}). Finally, more fibrils closer together are depicted for

the (3:1) blend ratio making the fullerene domains smaller and reducing the characteristic length as evidenced by the RSoXS analysis.

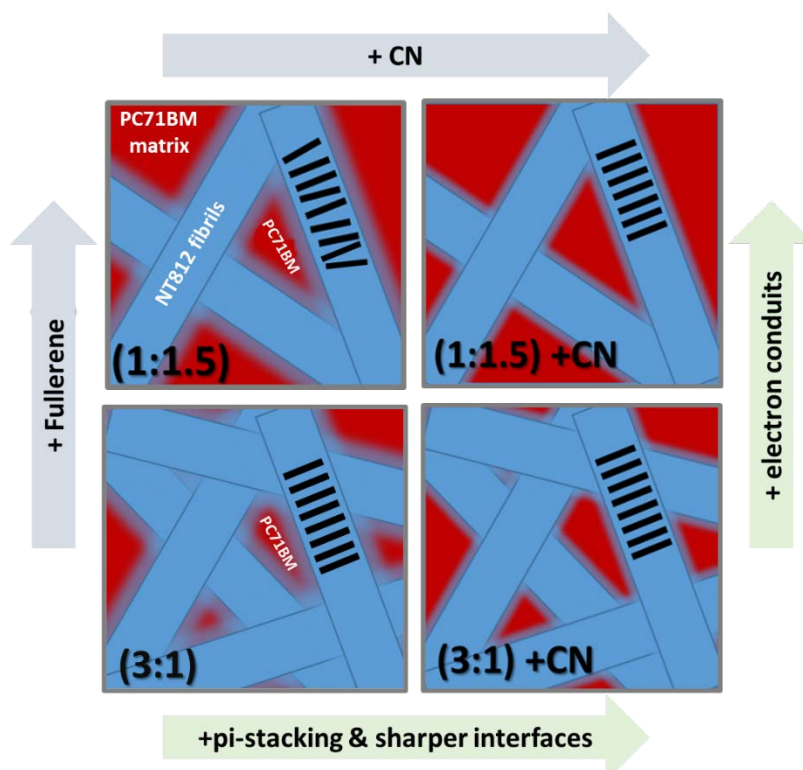


Figure 5. Depicted representation of morphology of OPV active layer in the investigated NT812:PC71BM blends. Polymer fibrils (blue) with stacked polymer chains (black) and matrix of fullerene (Red). We note that the fast growth direction of the fibril is unknown for this polymer and may not be the pi-stacking direction as is depicted here.

The question to be answered is what aspects of morphology are important to realize highly suppressed, non-Langevin recombination. In general, it has been found that domain purity in polymer based OSCs is important for device performance by aiding charge extraction and hindering recombination.^{22,24,50,51} This is likely an important prerequisite here, but the presence of pure domains in blends exhibiting both Langevin and non-Langevin recombination suggest this situation alone is insufficient. Venkatesan et al. have shown that charge recombination is high in low-performing polymer:fullerene systems with narrow domains despite good domain purity and conductivity.⁵² Our results go further to show that large and clean conduits to the electrodes keep charges from interacting with their counterparts in neighbouring domains,

whereas narrow pure domains increase the likelihood that charges will encounter each other or trap states at the interfaces. This is the most prevalent morphological change between the cells with Langevin versus non-Langevin recombination dynamics. Note that 25% PC71BM loading in the (3:1) blends, aggregating into pure phases, is well above the 3D percolation threshold, so although isolated-domain traps are possible,^{53,54} general fullerene domain connectivity should be no issue here.

A further clue to the importance of interfacial interaction comes from the correlation of sharpening interfaces rather than crystalline coherence with decreased recombination for both blend films. In particular, in (3:1) blends the recombination reduction factor γ more than doubles when interfacial mixing is reduced through the CN additive while there is no detectable change in crystallinity (GIWAXS) or aggregation (UV-Vis spectroscopy). The improvement in γ is not nearly as significant for the corresponding (1:1.5) blend devices, even though pi-stacking improves dramatically for them. We interpret this situation to mean that highly mixed or wide D-A interfaces can encroach on the charge pathways – especially when they are narrow – and enable holes and electrons to mingle and recombine in a way well-described by the Langevin model. Devices with large pure percolation pathways are more immune to interfacial details such that sharper interfaces are less critical for non-Langevin recombination.⁵⁵ The crystallinity improving with CN might also help in keeping holes toward the middle of transport conduits because the energy states in a well-delocalized crystal are lower than a defective crystal,⁵⁶ thus, resulting in even higher γ . Domain size must not be allowed to increase too far, however, due to the limitations of the exciton diffusion length (~20 nm). On top of suppressing recombination, there is increasing evidence that sharp interfaces are important for charge generation as well in semicrystalline systems.^{30,31} Thus, the highest efficiency devices will likely still depend on sharp interfaces and smaller domains to simultaneously harvest all excitons and transport charges.

Although we cannot conclusively say that perfectly discrete (zero width) interfaces are best, we have been able to uniquely remove the effects of domain purity and crystallinity/aggregation from the equation. Furthermore, our direct correlation to the Langevin reduction factor rather than short-circuit current enables us to eliminate possible influences of changing charge generation rates. Combined, these results reveal a definitive influence of interfacial sharpness on suppressing recombination.

To put our findings about the NT812 system into perspective, we compare it to the classical electron donor, poly3-hexylthiophene (P3HT), which exhibits non-Langevin recombination as well in fullerene based BHJ OSCs with thermal post-treatment.^{38,57,58} Both systems phase segregate in BHJ layers and result in pure fibrils at optimal fabrication conditions and both have similar charge carrier mobilities. In fact, fibrillar structures are good at purifying, sharpening, and limiting how large the domains get, so they do not get so big as to lower exciton dissociation efficiencies. However, the best NT812 OSCs' γ are higher than for P3HT devices (>1000 vs 100s). We attribute this to the fact that NT812, like many other polymers,^{59–61} has a stiffer and longer monomer than P3HT, which causes the NT812 fibrils to be wider resulting in larger charge conduits. On the other hand, there is significant room for improvement in NFAs, which now top OSC performance in thin layers but lose significant efficiency as thickness increases, even when processed to optimize aggregation.¹⁶ Therefore, more systems with NT812 type morphology are needed, namely with larger fibrils that strongly phase separate from the acceptor phase to result in sharp interfaces. Such a strategy will enable high efficiency devices with thicknesses >400 nm.

4. Conclusion

We have investigated the morphological mechanisms behind a novel high-performing polymer:fullerene OSC system known to exhibit both highly suppressed non-Langevin recombination and classical diffusive Langevin recombination dependent on the blend ratio. Our suite of synchrotron-based X-ray techniques were combined to reveal pure phases in all

preparation conditions, suggesting pure phases alone are not sufficient to realize non-Langevin recombination. Instead, we found that larger (>30 nm), pure, and well-aggregated domains with sharp D-A interfaces likely act as charge conduits across the active layers to effectively segregate charges and suppress bimolecular recombination via fast dissociation of charge transfer states for near-ideal charge generation and collection. Such morphological features are possible explanations to how efficient devices can be achieved with printable active layers up to $1\mu\text{m}$ in thickness. Thus, large, pure percolation pathways with sharp heterointerfaces may be required to achieve efficient OSCs suitable for large-scale industrial production.

5. Experimental Section

Device Fabrication:

The polymer (NT812) was supplied by Fei Huang in Institute of Polymer Optoelectronic Materials and Devices, South China University of Technology. The fullerene acceptor, PC71BM was purchased from Solenne. The solvents Chlorobenzene (CB) and 1,2-Dichlorobenzene (DCB), and the additive chloronaphthalene (CN) were purchased from Carl Roth and Alfa Aesar, respectively. The devices were fabricated with a conventional structure. First, the patterned indium tin oxide (ITO) glass substrates were cleaned in an ultrasonic bath with detergent, acetone, deionized water, and isopropyl alcohol and dried by nitrogen. The dried substrates were treated by oxygen plasma at room temperature for 4 min. Then PEDOT:PSS (purchased from Heraeus Deutschland (Clevios P AI4083)) was spin coated on top of the substrates (3000 rpm for 30 s, thickness of ≈ 30 nm) and the substrates were annealed at 150°C for 15 min in air. For deposition of active layers, blend solution of NT812 and PC71BM at a weight ratio of 1:1.5 and 3:1 dissolved in CB:DCB = 3:1 (with/without 0.5 vol % of CN) with total concentration of (20 mg ml^{-1}) were spin coated on top of PEDOT:PSS layer in a nitrogen filled glovebox. The blend films were annealed at 100°C for 15 min on a hot plate. After

cooling down, a 5 nm poly 9,9-bis6-(N,N,N-trimethylammonium) hexylfluorene-alt-co-phenylenebromide (PFN-Br) layer was spin coated from methanol solution onto the active layers. Finally, the films were transferred into a vacuum evaporator connected to the glovebox, and 100 nm silver was deposited sequentially through a shadow mask under ($\approx 1 \times 10^{-7}$ mbar), with an active area of the cells of ($A = 0.06 \text{ cm}^2$).

In order to prepare the films for morphology study, silicon wafers were cleaned as the ITO substrates cleaning process and then Na:PSS was spin coated (3000 rpm for 30 s) on top of it simulate the device PEDOT:PSS surface roughness and surface energy. The substrates were annealed at (150 °C) for (15 min) in air. The active layers were spin coated and then thermally annealed as described above.

Resistance-Dependent Photovoltage (RPV):

The devices were illuminated by a pulsed second harmonic Nd:YAG laser (NT242, EKSPLA) at 532 nm with 6 ns pulse duration. The laser intensity was attenuated with a normal optical density (OD) filter and set to the low intensity in order to prevent a redistribution (screening) of the internal electric field and maintaining quasi-short-circuit conditions regardless of the load resistance. Then the photocurrent and photovoltage transients were recorded by a digital storage oscilloscope (DSO9104H) via a LabVIEW code. Refer to previous work for more details about those techniques.⁷

Bias-assisted Charge Extraction (BACE):

To establish steady-state conditions, we used a high power (1 W, 638 nm) laser diode (insaneware) with a switch-off time of (10 ns). The laser diode was operated at (500 Hz) with a duty cycle of 50%, such that illumination lasted 1 ms and the diode was switched off for also 1 ms. A pulse generator (Agilent 81150A) was used to apply the prebias (V_{oc}) and collection bias which are amplified by a home-built amplifier, allowing a fast extraction time of (10-20

ns). The current transients were measured via a (10 Ω) resistor in series with the sample and recorded with an oscilloscope (Agilent DSO9104H).

Morphology Measurements:

To probe the active-layer nanomorphology in the investigated OPV systems, we utilized synchrotron-based X-ray microscopy, spectroscopy, and scattering techniques. GIWAXS, RSoXS and Spectroscopy/STXM were conducted at the Advanced Light Source, Berkeley, CA at beamlines 7.3.3,⁶² 11.0.1.2,⁶³ and 5.3.2,⁴² respectively. The morphologically examined active layers were prepared from the same batch as the examined OSC devices. GIWAXS data were taken at X-ray energy (10 KeV) and incident angle of (0.2 deg) (above the substrate critical angle) enabling intensities linear to the illuminated sample volume. Samples were spin coated on Na:PSS/Si. In addition to grazing incident angle (0.2 deg), a rocking scan was acquired around an incident angle of 10.55, which is the specular angle of the pi-pi scattering peak of the polymer. Additional angles of incidence were explored as well (e.g. 5.18, 7.72, 9.94 degrees). The data at 7.72 degree was used to patch up the missing wedge in the 0.2 degree data and to analyze for pole figures in a similar fashion to previous literature done Michael F. Toney et al.⁶⁴ RSoXS data were taken at X-ray energy below the C-edge at (283.5 eV). Samples were spin coated on Na:PSS/Si substrates then floated off in deionized water onto Si₃N₄ windows, low stress Si₃N₄ membrane with a size of (2 mm²) and thickness of (100 nm). RSoXS data were normalized to film thickness, which was measured via NEXAFS absorbance spectra acquired at the same position and where RSoXS was acquired and with the same X-ray beam. The RSoXS measurements were conducted in transmission mode at normal incidence, also at 45 degrees of sample tilt (see Figure S22).

STXM images, quantify chemical composition, were acquired at a fullerene resonant energy (284.4 eV) and non- resonant energy (320 eV). These energies were selected from

NEXAFS spectra for neat materials. All STXM and NEXAFS samples were spin coated on Na:PSS/Si substrates then floated off in deionized water onto TEM grids.

ASSOCIATED CONTENT

Supporting Information

The Supporting Information is available free of charge at (XXXXXX)

The Supporting Information is including detailed calculations of the D-A interfaces, more in-depth analysis of the X-ray measurements, and figures of the resistance-dependent photovoltage and bias-assisted charge extraction data (PDF)

AUTHOR INFORMATION

Corresponding Author

Brian A. Collins — Department of Physics and Astronomy, Washington State University, Pullman, WA 99164, USA; Materials Science and Engineering Program, Washington State University, Pullman WA 99164, USA, orcid.org/0000-0003-2047-8418; E-mail: brian.collins@wsu.edu;

Notes

The authors declare no competing financial interests.

ACKNOWLEDGMENT

Major funding for this work was provided by the US National Science Foundation DMR Electronic and Photonics Program under Grant #1905790 which also provided funding support for O.A. and T.M. The authors also acknowledge the Alexander von Humboldt Foundation (Sofja Kovalevskaja prize) for funding and Dieter Neher (PWM) for access to labs. Funding

support for T.F. and V.M. was provided by the US Department of Energy Early Career Research Program under Grant DE-SC0017923. This research used resources of the Advanced Light Source, which is a DOE Office of Science User facility under contract no. DE-AC02-05CH11231.

REFERENCES

- (1) Scharber, M. C.; Sariciftci, N. S. Efficiency of Bulk-Heterojunction Organic Solar Cells. *Progress in Polymer Science* **2013**, *38* (12), 1929–1940. <https://doi.org/10.1016/j.progpolymsci.2013.05.001>.
- (2) Liang, Y.; Feng, D.; Wu, Y.; Tsai, S.-T.; Li, G.; Ray, C.; Yu, L. Highly Efficient Solar Cell Polymers Developed via Fine-Tuning of Structural and Electronic Properties. *J. Am. Chem. Soc.* **2009**, *131* (22), 7792–7799. <https://doi.org/10.1021/ja901545q>.
- (3) Meng, L.; Zhang, Y.; Wan, X.; Li, C.; Zhang, X.; Wang, Y.; Ke, X.; Xiao, Z.; Ding, L.; Xia, R.; Yip, H.-L.; Cao, Y.; Chen, Y. Organic and Solution-Processed Tandem Solar Cells with 17.3% Efficiency. *Science* **2018**, *361* (6407), 1094–1098. <https://doi.org/10.1126/science.aat2612>.
- (4) Liu, Q.; Jiang, Y.; Jin, K.; Qin, J.; Xu, J.; Li, W.; Xiong, J.; Liu, J.; Xiao, Z.; Sun, K.; Yang, S.; Zhang, X.; Ding, L. 18% Efficiency Organic Solar Cells. *Science Bulletin* **2020**, *65* (4), 272–275. <https://doi.org/10.1016/j.scib.2020.01.001>.
- (5) Neher, D.; Kniepert, J.; Elimelech, A.; Koster, L. J. A. A New Figure of Merit for Organic Solar Cells with Transport-Limited Photocurrents. *Scientific Reports* **2016**, *6* (1), 24861. <https://doi.org/10.1038/srep24861>.
- (6) Bartesaghi, D.; Pérez, I. del C.; Kniepert, J.; Roland, S.; Turbiez, M.; Neher, D.; Koster, L. J. A. Competition between Recombination and Extraction of Free Charges Determines the Fill Factor of Organic Solar Cells. *Nat Commun* **2015**, *6* (1), 7083. <https://doi.org/10.1038/ncomms8083>.
- (7) Armin, A.; Chen, Z.; Jin, Y.; Zhang, K.; Huang, F.; Shoaee, S. A Shockley-Type Polymer: Fullerene Solar Cell. *Adv. Energy Mater.* **2018**, *8* (7), 1701450. <https://doi.org/10.1002/aenm.201701450>.
- (8) Duan, C.; Gao, K.; Colberts, F. J. M.; Liu, F.; Meskers, S. C. J.; Wienk, M. M.; Janssen, R. A. J. Thiophene Rings Improve the Device Performance of Conjugated Polymers in Polymer Solar Cells with Thick Active Layers. *Advanced Energy Materials* **2017**, *7* (19), 1700519. <https://doi.org/10.1002/aenm.201700519>.
- (9) Shoaee, S.; Armin, A.; Stolterfoht, M.; Hosseini, S. M.; Kurpiers, J.; Neher, D. Decoding Charge Recombination through Charge Generation in Organic Solar Cells. *Solar RRL* **2019**, *3* (11), 1900184. <https://doi.org/10.1002/solr.201900184>.
- (10) Gao, J.; Wang, J.; Xu, C.; Hu, Z.; Ma, X.; Zhang, X.; Niu, L.; Zhang, J.; Zhang, F. A Critical Review on Efficient Thick-Film Organic Solar Cells. *Solar RRL* **2020**, *4* (11), 2000364. <https://doi.org/10.1002/solr.202000364>.
- (11) Andersen, T. R.; Dam, H. F.; Hösel, M.; Helgesen, M.; Carlé, J. E.; Larsen-Olsen, T. T.; Gevorgyan, S. A.; Andreasen, J. W.; Adams, J.; Li, N.; Machui, F.; Spyropoulos, G. D.; Ameri, T.; Lemaître, N.; Legros, M.; Scheel, A.; Gaiser, D.; Kreul, K.; Berny, S.; Lozman, O. R.; Nordman, S.; Välimäki, M.; Vilkman, M.; Søndergaard, Roar. R.; Jørgensen, M.; Brabec, C. J.; Krebs, F. C. Scalable, Ambient Atmosphere Roll-to-Roll Manufacture of Encapsulated Large Area, Flexible Organic Tandem Solar Cell Modules. *Energy Environ. Sci.* **2014**, *7* (9), 2925. <https://doi.org/10.1039/C4EE01223B>.
- (12) Chang, Y.; Zhu, X.; Lu, K.; Wei, Z. Progress and Prospects of Thick-Film Organic Solar Cells. *J. Mater. Chem. A* **2021**, *9* (6), 3125–3150. <https://doi.org/10.1039/D0TA10594E>.
- (13) Jin, Y.; Chen, Z.; Dong, S.; Zheng, N.; Ying, L.; Jiang, X.-F.; Liu, F.; Huang, F.; Cao, Y. A Novel Naphtho[1,2-*c*:5,6-*C'*]Bis([1,2,5]Thiadiazole)-Based Narrow-Bandgap π -Conjugated Polymer with Power Conversion Efficiency Over 10%. *Adv. Mater.* **2016**, *28* (44), 9811–9818. <https://doi.org/10.1002/adma.201603178>.

- (14) Langevin, P. Recombinaison et Mobilites Des Ions Dans Les Gaz. *Ann. Chim. Phys* **1903**, No. 28, 433–530.
- (15) Ko, S.-J.; Walker, B.; Nguyen, T. L.; Choi, H.; Seifter, J.; Uddin, M. A.; Kim, T.; Kim, S.; Heo, J.; Kim, G.-H.; Cho, S.; Heeger, A. J.; Woo, H. Y.; Kim, J. Y. Photocurrent Extraction Efficiency near Unity in a Thick Polymer Bulk Heterojunction. *Advanced Functional Materials* **2016**, 26 (19), 3324–3330. <https://doi.org/10.1002/adfm.201505556>.
- (16) Hosseini, S. M.; Tokmoldin, N.; Lee, Y. W.; Zou, Y.; Woo, H. Y.; Neher, D.; Shoaee, S. Putting Order into PM6:Y6 Solar Cells to Reduce the Langevin Recombination in 400 Nm Thick Junction. *Solar RRL* **2020**, 4 (11), 2000498. <https://doi.org/10.1002/solr.202000498>.
- (17) Hosseini, S. M.; Roland, S.; Kurpiers, J.; Chen, Z.; Zhang, K.; Huang, F.; Armin, A.; Neher, D.; Shoaee, S. Impact of Bimolecular Recombination on the Fill Factor of Fullerene and Nonfullerene-Based Solar Cells: A Comparative Study of Charge Generation and Extraction. *J. Phys. Chem. C* **2019**, 123 (11), 6823–6830. <https://doi.org/10.1021/acs.jpcc.8b11669>.
- (18) Phuong, L. Q.; Hosseini, S. M.; Koh, C. W.; Woo, H. Y.; Shoaee, S. Measuring Competing Recombination Losses in a Significantly Reduced Langevin System by Steady-State Photoinduced Absorption and Photocurrent Spectroscopy. *J. Phys. Chem. C* **2019**, 123 (45), 27417–27422. <https://doi.org/10.1021/acs.jpcc.9b08901>.
- (19) Schwarz, K. N.; Geraghty, P. B.; Mitchell, V. D.; Khan, S.-U.-Z.; Sandberg, O. J.; Zarrabi, N.; Kudisch, B.; Subbiah, J.; Smith, T. A.; Rand, B. P.; Armin, A.; Scholes, G. D.; Jones, D. J.; Ghiggino, K. P. Reduced Recombination and Capacitor-like Charge Buildup in an Organic Heterojunction. *J. Am. Chem. Soc.* **2020**, 142 (5), 2562–2571. <https://doi.org/10.1021/jacs.9b12526>.
- (20) Murthy, D. H. K.; Melianas, A.; Tang, Z.; Juška, G.; Arlauskas, K.; Zhang, F.; Siebbeles, L. D. A.; Inganäs, O.; Savenije, T. J. Origin of Reduced Bimolecular Recombination in Blends of Conjugated Polymers and Fullerenes. *Adv. Funct. Mater.* **2013**, 23 (34), 4262–4268. <https://doi.org/10.1002/adfm.201203852>.
- (21) Pivrikas, A.; Sariciftci, N. S.; Juška, G.; Österbacka, R. A Review of Charge Transport and Recombination in Polymer/Fullerene Organic Solar Cells. *Progress in Photovoltaics: Research and Applications* **2007**, 15 (8), 677–696. <https://doi.org/10.1002/pip.791>.
- (22) Ye, L.; Hu, H.; Ghasemi, M.; Wang, T.; Collins, B. A.; Kim, J.-H.; Jiang, K.; Carpenter, J. H.; Li, H.; Li, Z.; McAfee, T.; Zhao, J.; Chen, X.; Lai, J. L. Y.; Ma, T.; Bredas, J.-L.; Yan, H.; Ade, H. Quantitative Relations between Interaction Parameter, Miscibility and Function in Organic Solar Cells. *Nature Mater* **2018**, 17 (3), 253–260. <https://doi.org/10.1038/s41563-017-0005-1>.
- (23) Yan, H.; Swaraj, S.; Wang, C.; Hwang, I.; Greenham, N. C.; Groves, C.; Ade, H.; McNeill, C. R. Influence of Annealing and Interfacial Roughness on the Performance of Bilayer Donor/Acceptor Polymer Photovoltaic Devices. *Advanced Functional Materials* **2010**, 20 (24), 4329–4337. <https://doi.org/10.1002/adfm.201001292>.
- (24) Lyons, B. P.; Clarke, N.; Groves, C. The Relative Importance of Domain Size, Domain Purity and Domain Interfaces to the Performance of Bulk-Heterojunction Organic Photovoltaics. *Energy Environ. Sci.* **2012**, 5 (6), 7657. <https://doi.org/10.1039/c2ee21327c>.
- (25) Zimmerman, J. D.; Xiao, X.; Renshaw, C. K.; Wang, S.; Diev, V. V.; Thompson, M. E.; Forrest, S. R. Independent Control of Bulk and Interfacial Morphologies of Small Molecular Weight Organic Heterojunction Solar Cells. *Nano Lett.* **2012**, 12 (8), 4366–4371. <https://doi.org/10.1021/nl302172w>.

- (26) McMahon, D. P.; Cheung, D. L.; Troisi, A. Why Holes and Electrons Separate So Well in Polymer/Fullerene Photovoltaic Cells. *J. Phys. Chem. Lett.* **2011**, 2 (21), 2737–2741. <https://doi.org/10.1021/jz201325g>.
- (27) Clarke, T. M.; Rodovsky, D. B.; Herzing, A. A.; Peet, J.; Dennler, G.; DeLongchamp, D.; Lungenschmied, C.; Mozer, A. J. Significantly Reduced Bimolecular Recombination in a Novel Silole-Based Polymer: Fullerene Blend. *Advanced Energy Materials* **2011**, 1 (6), 1062–1067. <https://doi.org/10.1002/aenm.201100390>.
- (28) Collins, B. A.; Li, Z.; Tumbleston, J. R.; Gann, E.; McNeill, C. R.; Ade, H. Absolute Measurement of Domain Composition and Nanoscale Size Distribution Explains Performance in PTB7:PC71BM Solar Cells. *Advanced Energy Materials* **2013**, 3 (1), 65–74. <https://doi.org/10.1002/aenm.201200377>.
- (29) Alqahtani, O.; Babics, M.; Gorenflot, J.; Savikhin, V.; Ferron, T.; Balawi, A. H.; Paulke, A.; Kan, Z.; Pope, M.; Clulow, A. J.; Wolf, J.; Burn, P. L.; Gentle, I. R.; Neher, D.; Toney, M. F.; Laquai, F.; Beaujuge, P. M.; Collins, B. A. Mixed Domains Enhance Charge Generation and Extraction in Bulk-Heterojunction Solar Cells with Small-Molecule Donors. *Adv. Energy Mater.* **2018**, 8 (19), 1702941. <https://doi.org/10.1002/aenm.201702941>.
- (30) Ferron, T.; Waldrip, M.; Pope, M.; Collins, B. A. Increased Charge Transfer State Separation via Reduced Mixed Phase Interface in Polymer Solar Cells. *J. Mater. Chem. A* **2019**, 7 (9), 4536–4548. <https://doi.org/10.1039/C8TA12336E>.
- (31) Dhakal, P.; Ferron, T.; Alotaibi, A.; Murcia, V.; Alqahtani, O.; Collins, B. A. Evidence for Field-Dependent Charge Separation Caused by Mixed Phases in Polymer–Fullerene Organic Solar Cells. *J. Phys. Chem. Lett.* **2021**.
- (32) Venkatesan, S.; Chen, J.; Ngo, E. C.; Dubey, A.; Khatiwada, D.; Zhang, C.; Qiao, Q. Critical Role of Domain Crystallinity, Domain Purity and Domain Interface Sharpness for Reduced Bimolecular Recombination in Polymer Solar Cells. *Nano Energy* **2015**, 12, 457–467. <https://doi.org/10.1016/j.nanoen.2014.12.027>.
- (33) Ye, L.; Zhang, S.; Ma, W.; Fan, B.; Guo, X.; Huang, Y.; Ade, H.; Hou, J. From Binary to Ternary Solvent: Morphology Fine-Tuning of D/A Blends in PDPP3T-Based Polymer Solar Cells. *Advanced Materials* **2012**, 24 (47), 6335–6341. <https://doi.org/10.1002/adma.201202855>.
- (34) Vandewal, K.; Gadisa, A.; Oosterbaan, W. D.; Bertho, S.; Banishoeib, F.; Van Severen, I.; Lutsen, L.; Cleij, T. J.; Vanderzande, D.; Manca, J. V. The Relation Between Open-Circuit Voltage and the Onset of Photocurrent Generation by Charge-Transfer Absorption in Polymer : Fullerene Bulk Heterojunction Solar Cells: Photocurrent Generation by Charge-Transfer Absorption. *Adv. Funct. Mater.* **2008**, 18 (14), 2064–2070. <https://doi.org/10.1002/adfm.200800056>.
- (35) Stolterfoht, M.; Armin, A.; Shoaee, S.; Kassal, I.; Burn, P.; Meredith, P. Slower Carriers Limit Charge Generation in Organic Semiconductor Light-Harvesting Systems. *Nat Commun* **2016**, 7 (1), 11944. <https://doi.org/10.1038/ncomms11944>.
- (36) Armin, A.; Juska, G.; Ullah, M.; Velusamy, M.; Burn, P. L.; Meredith, P.; Pivrikas, A. Balanced Carrier Mobilities: Not a Necessary Condition for High-Efficiency Thin Organic Solar Cells as Determined by MIS-CELIV. *Advanced Energy Materials* **2014**, 4 (4), 1300954. <https://doi.org/10.1002/aenm.201300954>.
- (37) Zhang, K.; Chen, Z.; Armin, A.; Dong, S.; Xia, R.; Yip, H.-L.; Shoaee, S.; Huang, F.; Cao, Y. Efficient Large Area Organic Solar Cells Processed by Blade-Coating With Single-Component Green Solvent. *Solar RRL* **2018**, 2 (1), 1700169. <https://doi.org/10.1002/solr.201700169>.
- (38) Armin, A.; Subbiah, J.; Stolterfoht, M.; Shoaee, S.; Xiao, Z.; Lu, S.; Jones, D. J.; Meredith, P. Reduced Recombination in High Efficiency Molecular Nematic Liquid

- Crystalline: Fullerene Solar Cells. *Advanced Energy Materials* **2016**, 6 (22), 1600939. <https://doi.org/10.1002/aenm.201600939>.
- (39) Rivnay, J.; Mannsfeld, S. C. B.; Miller, C. E.; Salleo, A.; Toney, M. F. Quantitative Determination of Organic Semiconductor Microstructure from the Molecular to Device Scale. *Chem. Rev.* **2012**, 112 (10), 5488–5519. <https://doi.org/10.1021/cr3001109>.
 - (40) Richter, L. J.; DeLongchamp, D. M.; Amassian, A. Morphology Development in Solution-Processed Functional Organic Blend Films: An In Situ Viewpoint. *Chem. Rev.* **2017**, 117 (9), 6332–6366. <https://doi.org/10.1021/acs.chemrev.6b00618>.
 - (41) Li, Z.; Jiang, K.; Yang, G.; Lai, J. Y. L.; Ma, T.; Zhao, J.; Ma, W.; Yan, H. Donor Polymer Design Enables Efficient Non-Fullerene Organic Solar Cells. *Nat Commun* **2016**, 7 (1), 13094. <https://doi.org/10.1038/ncomms13094>.
 - (42) Kilcoyne, A. L. D.; Tylliszczak, T.; Steele, W. F.; Fakra, S.; Hitchcock, P.; Franck, K.; Anderson, E.; Harteneck, B.; Rightor, E. G.; Mitchell, G. E.; Hitchcock, A. P.; Yang, L.; Warwick, T.; Ade, H. Interferometer-Controlled Scanning Transmission X-Ray Microscopes at the Advanced Light Source. *J Synchrotron Rad* **2003**, 10 (2), 125–136. <https://doi.org/10.1107/S0909049502017739>.
 - (43) Collins, B. A.; Ade, H. Quantitative Compositional Analysis of Organic Thin Films Using Transmission NEXAFS Spectroscopy in an X-Ray Microscope. *Journal of Electron Spectroscopy and Related Phenomena* **2012**, 185 (5–7), 119–128. <https://doi.org/10.1016/j.elspec.2012.05.002>.
 - (44) Collins, B. A.; Gann, E. Resonant Soft X-Ray Scattering in Polymer Science. *Journal of Polymer Science n/a* (n/a). <https://doi.org/10.1002/pol.20210414>.
 - (45) Tumbleston, J. R.; Collins, B. A.; Yang, L.; Stuart, A. C.; Gann, E.; Ma, W.; You, W.; Ade, H. The Influence of Molecular Orientation on Organic Bulk Heterojunction Solar Cells. *Nature Photon* **2014**, 8 (5), 385–391. <https://doi.org/10.1038/nphoton.2014.55>.
 - (46) Ferron, T.; Pope, M.; Collins, B. A. Spectral Analysis for Resonant Soft X-Ray Scattering Enables Measurement of Interfacial Width in 3D Organic Nanostructures. *Phys. Rev. Lett.* **2017**, 119 (16), 167801. <https://doi.org/10.1103/PhysRevLett.119.167801>.
 - (47) Kozub, D. R.; Vakhshouri, K.; Orme, L. M.; Wang, C.; Hexemer, A.; Gomez, E. D. Polymer Crystallization of Partially Miscible Polythiophene/Fullerene Mixtures Controls Morphology. *Macromolecules* **2011**, 44 (14), 5722–5726. <https://doi.org/10.1021/ma200855r>.
 - (48) Pfannmöller, M.; Flügge, H.; Benner, G.; Wacker, I.; Sommer, C.; Hanselmann, M.; Schmale, S.; Schmidt, H.; Hamprecht, F. A.; Rabe, T.; Kowalsky, W.; Schröder, R. R. Visualizing a Homogeneous Blend in Bulk Heterojunction Polymer Solar Cells by Analytical Electron Microscopy. *Nano Lett.* **2011**, 11 (8), 3099–3107. <https://doi.org/10.1021/nl201078t>.
 - (49) Guo, C.; Kozub, D. R.; Vajjala Kesava, S.; Wang, C.; Hexemer, A.; Gomez, E. D. Signatures of Multiphase Formation in the Active Layer of Organic Solar Cells from Resonant Soft X-Ray Scattering. *ACS Macro Lett.* **2013**, 2 (3), 185–189. <https://doi.org/10.1021/mz300547x>.
 - (50) Mukherjee, S.; Proctor, C. M.; Tumbleston, J. R.; Bazan, G. C.; Nguyen, T.-Q.; Ade, H. Importance of Domain Purity and Molecular Packing in Efficient Solution-Processed Small-Molecule Solar Cells. *Adv. Mater.* **2015**, 27 (6), 1105–1111. <https://doi.org/10.1002/adma.201404388>.
 - (51) Albrecht, S.; Schindler, W.; Kurpiers, J.; Kniepert, J.; Blakesley, J. C.; Dumsch, I.; Allard, S.; Fostiropoulos, K.; Scherf, U.; Neher, D. On the Field Dependence of Free Charge Carrier Generation and Recombination in Blends of PCPDTBT/PC₇₀BM: Influence of Solvent Additives. *J. Phys. Chem. Lett.* **2012**, 3 (5), 640–645. <https://doi.org/10.1021/jz3000849>.

- (52) Venkatesan, S.; Adhikari, N.; Chen, J.; Ngo, E. C.; Dubey, A.; Galipeau, D. W.; Qiao, Q. Interplay of Nanoscale Domain Purity and Size on Charge Transport and Recombination Dynamics in Polymer Solar Cells. *Nanoscale* **2014**, *6* (2), 1011–1019. <https://doi.org/10.1039/C3NR05177C>.
- (53) Erb, T.; Zhokhavets, U.; Gobsch, G.; Raleva, S.; Stühn, B.; Schilinsky, P.; Waldauf, C.; Brabec, C. J. Correlation Between Structural and Optical Properties of Composite Polymer/Fullerene Films for Organic Solar Cells. *Adv. Funct. Mater.* **2005**, *15* (7), 1193–1196. <https://doi.org/10.1002/adfm.200400521>.
- (54) Solanki, A.; Wu, B.; Salim, T.; Lam, Y. M.; Sum, T. C. Correlation between Blend Morphology and Recombination Dynamics in Additive-Added P3HT:PCBM Solar Cells. *Phys. Chem. Chem. Phys.* **2015**, *17* (39), 26111–26120. <https://doi.org/10.1039/C5CP03762J>.
- (55) Vohra, V.; Kawashima, K.; Kakara, T.; Koganezawa, T.; Osaka, I.; Takimiya, K.; Murata, H. Efficient Inverted Polymer Solar Cells Employing Favourable Molecular Orientation. *Nature Photon* **2015**, *9* (6), 403–408. <https://doi.org/10.1038/nphoton.2015.84>.
- (56) Jamieson, F. C.; Domingo, E. B.; McCarthy-Ward, T.; Heeney, M.; Stingelin, N.; Durrant, J. R. Fullerenecrystallisation as a Key Driver of Charge Separation in Polymer/Fullerene Bulk Heterojunction Solar Cells. *Chem. Sci.* **2012**, *3* (2), 485–492. <https://doi.org/10.1039/C1SC00674F>.
- (57) Szymtkowski, J. On the Tendency of Temperature and Electric Field Dependences of Interface Recombination in a P3HT:PCBM Organic Bulk Heterojunction Solar Cell. *Semicond. Sci. Technol.* **2011**, *26* (10), 105012. <https://doi.org/10.1088/0268-1242/26/10/105012>.
- (58) Gorenflot, J.; Heiber, M. C.; Baumann, A.; Lorrman, J.; Gunz, M.; Kämpgen, A.; Dyakonov, V.; Deibel, C. Nongeminate Recombination in Neat P3HT and P3HT:PCBM Blend Films. *Journal of Applied Physics* **2014**, *115* (14), 144502. <https://doi.org/10.1063/1.4870805>.
- (59) Awartani, O.; Lemanski, B. I.; Ro, H. W.; Richter, L. J.; DeLongchamp, D. M.; O'Connor, B. T. Correlating Stiffness, Ductility, and Morphology of Polymer:Fullerene Films for Solar Cell Applications. *Advanced Energy Materials* **2013**, *3* (3), 399–406. <https://doi.org/10.1002/aenm.201200595>.
- (60) Do, K.; Huang, D. M.; Faller, R.; Moulé, A. J. A Comparative MD Study of the Local Structure of Polymer Semiconductors P3HT and PBTTT. *Phys. Chem. Chem. Phys.* **2010**, *12* (44), 14735. <https://doi.org/10.1039/c0cp00785d>.
- (61) Feng, S.; Zhang, C.; Liu, Y.; Bi, Z.; Zhang, Z.; Xu, X.; Ma, W.; Bo, Z. Fused-Ring Acceptors with Asymmetric Side Chains for High-Performance Thick-Film Organic Solar Cells. *Adv. Mater.* **2017**, *29* (42), 1703527. <https://doi.org/10.1002/adma.201703527>.
- (62) Hexemer, A.; Bras, W.; Glossinger, J.; Schaible, E.; Gann, E.; Kirian, R.; MacDowell, A.; Church, M.; Rude, B.; Padmore, H. A SAXS/WAXS/GISAXS Beamline with Multilayer Monochromator. *J. Phys.: Conf. Ser.* **2010**, *247*, 012007. <https://doi.org/10.1088/1742-6596/247/1/012007>.
- (63) Gann, E.; Young, A. T.; Collins, B. A.; Yan, H.; Nasiatka, J.; Padmore, H. A.; Ade, H.; Hexemer, A.; Wang, C. Soft X-Ray Scattering Facility at the Advanced Light Source with Real-Time Data Processing and Analysis. *Review of Scientific Instruments* **2012**, *83* (4), 045110. <https://doi.org/10.1063/1.3701831>.
- (64) Baker, J. L.; Jimison, L. H.; Mannsfeld, S.; Volkman, S.; Yin, S.; Subramanian, V.; Salleo, A.; Alivisatos, A. P.; Toney, M. F. Quantification of Thin Film Crystallographic Orientation Using X-Ray Diffraction with an Area Detector. *Langmuir* **2010**, *26* (11), 9146–9151. <https://doi.org/10.1021/la904840q>.

TOC GRAPHICS

